times of many hours, single-photon emission in our system can be maintained for even longer periods.

In most of the measurements reported here, we chose the length of the pump pulses to optimize the single-photon output rate[24]. By using slightly slower pulses and suitable detuning and intensity of the pump beam, we achieved a single-photon efficiency of $(8.0 \pm 1.3)\%$, in accordance with theoretical calculations[24]. For the remaining 92% of the pump pulses, an infrared fluorescence photon is radiated to the side of the cavity. Note that these incoherent emission events, while reducing the efficiency of single-photon generation, do not affect the waveform of the photons emanating from the cavity. The reason is that for off-resonant Raman-coupling of the $P_{1/2}$ and $D_{3/2}$ levels, cavity emission only occurs as a result of coherent evolution.

The efficiency can be substantially increased by reducing the cavity length. When the coupling is sufficiently strong, our system constitutes a high-fidelity interface between internal quantum states of localized ions and propagating photonic states. This is an essential tool for linking quantum information processing sites in a quantum network. □

Methods

The APDs we have used in evaluating the performance of our single-photon source have a large single-photon detection efficiency of 30% at 866 nm, but suffer from a non-negligible dark-count rate of approximately $50\,s^{-1}$. Although it is straightforward to subtract the dark-count-related background in the pulse-shape measurements of Fig. 2, the elimination of dark-count events from the correlation data requires a more elaborate procedure. If, in addition to the real photon counts $p_1(t)$ and $p_2(t)$ in the two detectors at time t, dark-count events $d_1(t)$ and $d_2(t)$ occur, the following identity holds for two-channel correlation functions:

$$\langle p_1(t+\tau)p_2(t)\rangle = \langle [p_1(t+\tau)+d_1(t+\tau)][p_2(t)+d_2(t)]\rangle - \langle d_1(t+\tau)[p_2(t)+d_2(t)]\rangle - \langle [p_1(t+\tau)+d_1(t+\tau)]d_2(t)\rangle + \langle d_1(t+\tau)d_2(t)\rangle \quad (1)$$

We determined the required correlation function $\langle p_1(t+\tau)p_2(t)\rangle$ according to equation (1) by evaluating cross-correlations between our dark-count-affected data sets ($p_1 + d_1$ or $p_2 + d_2$) and time records of dark counts only (d_1 or d_2), measured with no ion present in the trap. These reference measurements were taken immediately following the acquisition of the single-photon data. Because we averaged over a long measurement time, equation (1) is valid even though signal counts and dark counts were recorded subsequently. The four correlation measurements that were evaluated to obtain Fig. 3 are presented individually in the Supplementary Fig. 1. We took into account fluctuations of the dark-count rate by averaging over 400 different dark-count histories, unambiguously removing their contribution from the photon correlation measurements shown in Figs 3 and 4.

Received 12 May; accepted 18 August 2004; doi:10.1038/nature02961.

1. Bennett, C. H. & Brassard, G. *Proc. IEEE Int. Conf. on Computers, Systems, and Signal Processing (Bangalore, India)* 175–179 (IEEE, New York, 1984).
2. Knill, E., Laflamme, R. & Milburn, G. J. A scheme for efficient quantum computation with linear optics. *Nature* **409,** 46–52 (2001).
3. Diedrich, F. & Walther, H. Nonclassical radiation of a single stored ion. *Phys. Rev. Lett.* **58,** 203–206 (1987).
4. Basché, T., Moerner, W. E., Orrit, M. & Talon, H. Photon antibunching in the fluorescence of a single dye molecule trapped in a solid. *Phys. Rev. Lett.* **69,** 1516–1519 (1992).
5. Lounis, B. & Moerner, W. E. Single photons on demand from a single molecule at room temperature. *Nature* **407,** 491–493 (2000).
6. Kurtsiefer, C., Mayer, S., Zarda, P. & Weinfurter, H. Stable solid-state source of single photons. *Phys. Rev. Lett.* **85,** 290–293 (2000).
7. Brouri, R., Beveratos, A., Poizat, J.-P. & Grangier, P. Photon antibunching in the fluorescence of individual color centers in diamond. *Opt. Lett.* **25,** 1294–1296 (2000).
8. Michler, P. *et al.* A quantum dot single-photon turnstile device. *Science* **290,** 2282–2286 (2000).
9. Santori, C., Pelton, M., Solomon, G., Dale, Y. & Yamamoto, Y. Triggered single photons from a quantum dot. *Phys. Rev. Lett.* **86,** 1502–1505 (2001).
10. Moreau, E. *et al.* Single-mode solid-state single photon source based on isolated quantum dots in pillar microcavities. *Appl. Phys. Lett.* **79,** 2865–2867 (2001).
11. Yuan, Z. L. *et al.* Electrically driven single-photon source. *Science* **295,** 102–105 (2002).
12. Santori, C., Fattal, D., Vučković, J., Solomon, G. S. & Yamamoto, Y. Indistinguishable photons from a single-photon device. *Nature* **419,** 594–597 (2002).
13. Cirac, J. I., Zoller, P., Kimble, H. J. & Mabuchi, H. Quantum state transfer and entanglement distribution among distant nodes in a quantum network. *Phys. Rev. Lett.* **78,** 3221–3224 (1997).
14. Kuhn, A., Hennrich, M. & Rempe, G. Deterministic single-photon source for distributed quantum networking. *Phys. Rev. Lett.* **89,** 67901 (2002).
15. McKeever, J. *et al.* Deterministic generation of single photons from one atom trapped in a cavity. *Science* **303,** 1992–1994 (2004).
16. Brattke, S., Varcoe, B. T. H. & Walther, H. Generation of photon number states on demand via cavity quantum electrodynamics. *Phys. Rev. Lett.* **86,** 3534–3537 (2001).
17. Law, C. K. & Kimble, H. J. Deterministic generation of a bit-stream of single-photon pulses. *J. Mod. Opt.* **44,** 2067–2074 (1997).
18. Duan, L.-M., Kuzmich, A. & Kimble, H. J. Cavity QED and quantum-information processing with "hot" trapped atoms. *Phys. Rev. A.* **67,** 032305 (2003).
19. Pellizzari, T., Gardiner, S. A., Cirac, J. I. & Zoller, P. Decoherence, continuous observation, and quantum computing—a cavity QED model. *Phys. Rev. Lett.* **75,** 3788–3791 (1995).
20. Beige, A., Braun, D., Tregenna, B. & Knight, P. L. Quantum computing using dissipation to remain in a decoherence-free subspace. *Phys. Rev. Lett.* **85,** 1762–1765 (2000).
21. Zheng, S. B. & Guo, G. C. Efficient scheme for two-atom entanglement and quantum information processing in cavity QED. *Phys. Rev. Lett.* **85,** 2392–2395 (2000).
22. Guthöhrlein, G. R., Keller, M., Hayasaka, K., Lange, W. & Walther, H. A single ion as a nanoscopic probe of an optical field. *Nature* **414,** 49–51 (2001).
23. Keller, M., Lange, B., Hayasaka, K., Lange, W. & Walther, H. Deterministic coupling of single ions to an optical cavity. *Appl. Phys. B* **76,** 125–128 (2003).
24. Keller, M., Lange, B., Hayasaka, K., Lange, W. & Walther, H. A calcium ion in a cavity as a controlled single-photon source. *New J. Phys.* **6,** 95 (2004); available at http://www.iop.org/EJ/abstract/1367-2630/6/1/095.
25. Brendel, J., Tittel, W., Zbinden, H. & Gisin, N. Pulsed energy-time entangled twin-photon source for quantum communication. *Phys. Rev. Lett.* **82,** 2594–2597 (1999).

Supplementary Information accompanies the paper on **www.nature.com/nature**.

Acknowledgements We gratefully acknowledge the financial support of the European Commission through the QUEST, QUBITS and QGATES networks.

Competing interests statement The authors declare that they have no competing financial interests.

Correspondence and requests for materials should be addressed to W.L. (Wolfgang.Lange@mpq.mpg.de).

Crystallization of charge holes in the spin ladder of $Sr_{14}Cu_{24}O_{41}$

P. Abbamonte[1,2], G. Blumberg[3], A. Rusydi[1,4], A. Gozar[3,5], P. G. Evans[6], T. Siegrist[3], L. Venema[4], H. Eisaki[7], E. D. Isaacs[3,8] & G. A. Sawatzky[9]

[1]*National Synchrotron Light Source, Brookhaven National Laboratory, Upton, New York 11973, USA*
[2]*Department of Physics and Astronomy, SUNY Stony Brook, Stony Brook, New York 11794, USA*
[3]*Bell Laboratories, Lucent Technologies, Murray Hill, New Jersey 07974, USA*
[4]*University of Groningen, 9747 AG Groningen, The Netherlands*
[5]*Department of Physics, University of Illinois at Urbana-Champaign, Urbana, Illinois 61801, USA*
[6]*Department of Materials Science & Engineering, University of Wisconsin, Madison, Wisconsin 53706, USA*
[7]*Nanoelectronics Research Institute, AIST, 1-1-1 Central 2, Umezono, Tsukuba, Ibaraki, 305-8568, Japan*
[8]*Center for Nanoscale Materials, Argonne National Laboratory, Argonne, Illinois 60439, USA*
[9]*Department of Physics and Astronomy, University of British Columbia, Vancouver, British Columbia V6T-1Z1, Canada*

Determining the nature of the electronic phases that compete with superconductivity in high-transition-temperature (high-T_c) superconductors is one of the deepest problems in condensed matter physics. One candidate is the 'stripe' phase[1–3], in which the charge carriers (holes) condense into rivers of charge that separate regions of antiferromagnetism. A related but lesser known system is the 'spin ladder', which consists of two coupled chains of magnetic ions forming an array of rungs. A doped ladder can be thought of as a high-T_c material with lower dimensionality, and has been predicted to exhibit both superconductivity[4–6] and an insulating 'hole crystal'[4,7,8] phase in which the carriers are localized through many-body interactions. The competition between the two resembles that believed to operate between stripes and superconductivity in high-T_c materials[9]. Here we report the existence of a hole crystal in the doped spin ladder of $Sr_{14}Cu_{24}O_{41}$ using a resonant X-ray scattering technique[10]. This phase exists without a detectable distortion in the

structural lattice, indicating that it arises from many-body electronic effects. Our measurements confirm theoretical predictions[4,7,8], and support the picture that proximity to charge ordered states is a general property of superconductivity in copper oxides.

$Sr_{14}Cu_{24}O_{41}$ (SCO) is a layered material consisting of two different types of copper oxide sheets—a CuO_2 'chain' layer and a Cu_2O_3 'ladder' layer (see ref. 11 for a picture). These two sublayers are separated by Sr atoms, and stack in an alternating fashion along the *b* crystallographic direction. The ladders and chains are parallel and run along the *c* direction, but are structurally incommensurate; that is, the ratio of their lattice parameters, $c_L/c_c = \sqrt{2}$, is not a rational number. As a result SCO is internally strained, and has a large unit cell with low-temperature lattice parameters $a = 11.47$ Å, $b = 13.35$ Å, $c = 27.3$ Å $\approx 7c_L \approx 10c_c$ (ref. 12).

SCO is an intrinsically hole-doped material with 6 hole carriers per formula unit, of which 5.2 reside in the chain layer and 0.8 in the ladder[13]. SCO has the striking property that, when alloyed with Ca and subjected to a hydrostatic pressure of 3 GPa, it superconducts with $T_c = 12$ K (ref. 14). Without Ca, however, it exhibits all the transport signatures of a charge density wave (CDW), including a screening mode in impedance measurements[15,16], a pinning mode in microwave conductivity[17], a giant dielectric constant[15,16], and a nonlinear current–voltage (*I*–*V*) curve[15], which together indicate that the carrier density is modulated in real space. These observations are typical of conventional Peierls CDW materials like $NbSe_3$ or $K_{0.3}MoO_3$ (ref. 18) in which the carrier density is modulated by a distortion in the crystal structure, driven by the electron–lattice interaction. However, a hole crystal, which is expected to compete with superconductivity in doped ladders and is driven instead by many-body interactions, would bear these same signatures. Could $Sr_{14}Cu_{24}O_{41}$ contain a hole crystal?

Distinguishing between the two requires determining whether the modulation is tied to a lattice distortion or occurs only among the carriers (though perhaps influencing the lattice indirectly). Recently we demonstrated that resonant X-ray scattering[10] at energies near the K shell of oxygen ($1s \rightarrow 2p$ transition) is directly sensitive to hole ordering. In this method, the X-ray energy is tuned to the oxygen mobile carrier prepeak (MCP, see Fig. 1) at which scattering from the holes is selectively enhanced by $>10^3$. Here we apply this technique to search for hole ordering in SCO. This material is a particularly interesting case because it has hole carriers in both the ladder and chain layers, and the MCP is split into resolvable ladder and chain features[13]. Each provides a separate enhancement, permitting ordering in two layers to be distinguished.

Single crystals of SCO were grown by travelling solvent floating zone techniques[19], cut to (0,0,1) orientation, polished with diamond film down to 0.1 μm roughness, and annealed in O_2 at 120 °C to condition the surface. Resonant soft X-ray scattering (RSXS) measurements were carried out on the X1B undulator line at the National Synchrotron Light Source with a 10-axis, ultrahigh-vacuum diffractometer. Here we will use the Miller indices *H* and *K* to

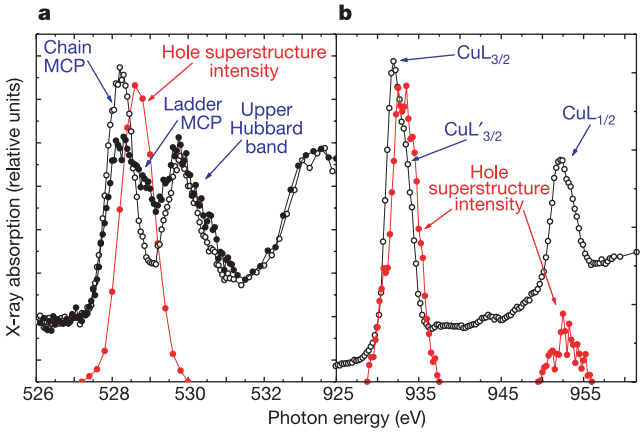

Figure 1 Energy dependence of the hole superstructure reflection compared to X-ray absorption spectra. Black symbols, absorption spectra of $Sr_{14}Cu_{24}O_{41}$, taken *in situ* in fluorescence-yield mode, in the vicinity of **a**, the oxygen K edge, which is a $1s \rightarrow 2p$ transition, and **b**, copper $L_{3/2,1/2}$ edges, which are $2p \rightarrow 3d$ transitions where the core hole is left with its spin either parallel ($j = 3/2$) or antiparallel ($j = 1/2$) to its orbital moment. Open circles, data taken with the photon polarization **E**||**a**; filled circles, data taken with approximately **E**||**c**. The data are in good agreement with ref. 13. "Chain MCP" and "ladder MCP" indicate the respective oxygen mobile carrier prepeaks (MCP) where scattering from the holes is enhanced. Red symbols, integrated intensity of the hole superstructure reflection as a function of incident photon energy. The reflection is visible only when the X-ray energy is tuned to the ladder MCP or the copper $L'_{3/2}$ ligand hole sideband, indicating the presence of a standing wave in the hole density in the ladder.

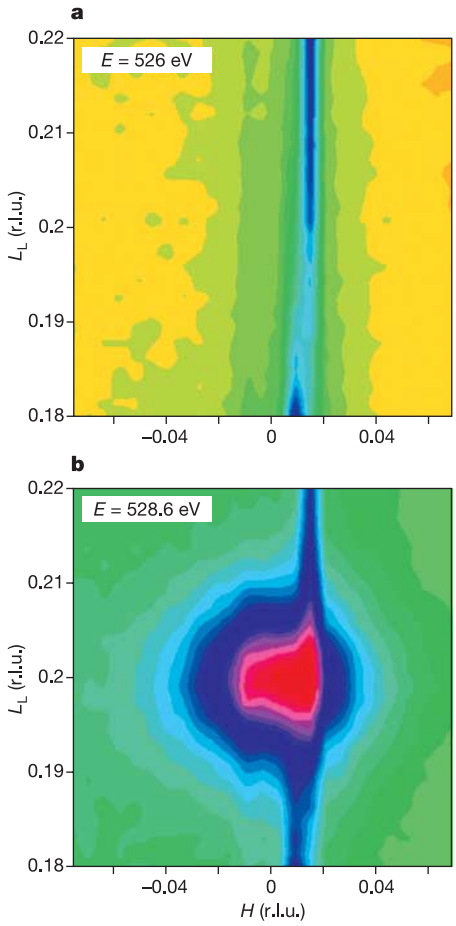

Figure 2 Appearance of the hole superstructure peak on resonance. **a**, Off-resonance ($E = 526$ eV) reciprocal space map around $(H,K,L_L) = (0,0,0.2)$. The 'rod' at $H = 0.01$ is the specular reflectance from the surface, which is displaced from $H = 0$ because of surface miscut. The width of this rod indicates our transverse momentum resolution. **b**, Same reciprocal space region with the X-ray energy tuned to the ladder MCP ($E = 528.6$ eV). A pronounced superlattice reflection appears at $L_L = 0.200 \pm 0.009$, indicating the presence of a commensurate standing wave in the ladder hole density with period $\lambda = 5.00c_L$. This reflection indexes to neither the 27.3 Å unit cell nor the previously reported chain dimerization reflections[11,12,21,22]. The peak width gives longitudinal and transverse coherence lengths of $\xi_c = 255$ Å $= 65.3c_L$ and $\xi_a = 274$ Å $= 24.9a$, respectively. The hole modulation is registered across 50 neighbouring ladders, indicating significant inter-ladder coupling in this system. r.l.u., reciprocal lattice units.

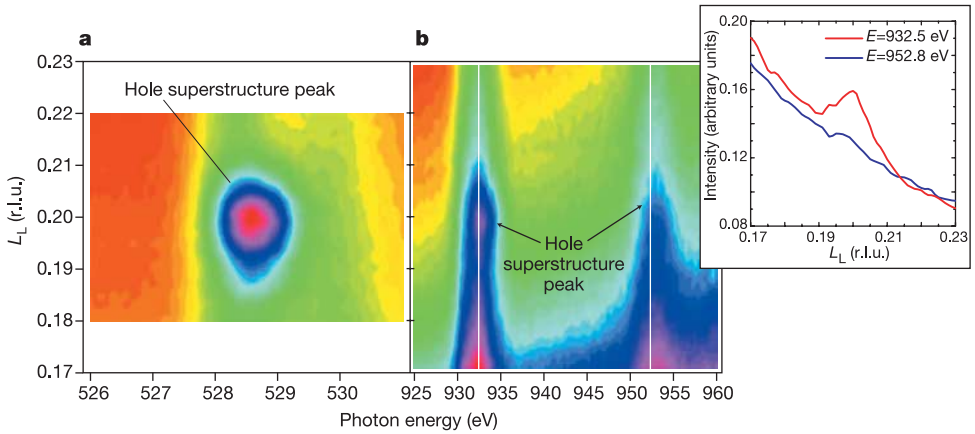

Figure 3 Energy- and L_L-dependence of the hole superstructure reflection. **a**, **b**, Peak intensity and L_L position across the oxygen K edge (**a**) and the copper $L_{3/2}$ and $L_{1/2}$ edges (**b**). The hole crystal reflection is clearly visible at both the ladder MCP (Bragg angle = 36.1°) and the copper $L_{3/2}$ edge (Bragg angle = 19.9°). In both cases it resides at $L_L = 0.200$, indicating that, although visible only at select energies, the reflection nonetheless disperses according to Bragg's law. This establishes it as a coherent, bulk phenomenon. The background in **b** is from the specular surface reflection, which is strong at the copper L edge. Inset, L_L scans on the $L_{3/2}$ (932.5 eV) and $L_{1/2}$ (952.8 eV) peaks, corresponding to the sections indicated with white lines.

denote periodicities along the a and b directions, respectively. For the c direction we will respectively use L_c, L_L and L to denote periodicity in terms of reciprocal units of the chain, ladder, and total unit cell, that is, $L = 7L_L = 10L_c$.

Previous studies of SCO with inelastic neutron scattering[20] have reported evidence for a spin dimerization in the chain layer with a periodicity of $5c_c$. This has been corroborated by neutron[12], X-ray[11,21] and electron[22] diffraction, which have shown 'superlattice' Bragg reflections that index roughly as $L_c = 2n \pm 0.2$ (refs 11, 12). This phenomenon is unlikely to account for the observed CDW transport properties, however, since transport in this system is determined by the ladders[23]. Moreover, in terms of the true unit cell these reflections index as $L = 20n \pm 2$ (always an integer), and so are not superlattice reflections in the true sense[12,24]. So far, no true superlattice, with a periodicity different from the 27.3 Å unit cell, has been observed in this material.

In Fig. 2 we show reciprocal space maps around $(H,K,L_L) = (0,0,0.2)$ at $T = 28$ K, for X-ray energies both off and on the MCP of the ladder. Off resonance, only a specular 'rod' is visible, due to reflectance from the sample surface. If tuned to the ladder MCP, however, a pronounced superlattice reflection appears, centred at $(H,K,L_L) = (0,0,0.200 \pm 0.009)$, indicating the existence of a modulation along the ladder with period $5.00 \pm 0.24\ c_L$. This reflection is commensurate but is truly a superlattice peak, because it occurs at $L = 1.4$ (or $L_c = 0.14$) and so does not have the periodicity of the 27.3 Å unit cell. In particular, it should not be confused with the chain dimerization reflections, which have a different periodicity.

Our central observation is the extremely unusual energy dependence of this peak. It was tracked through the oxygen K edge where it was found to be visible only for incident energies in resonance with the ladder MCP (Fig. 1)—an observation reproduced in two samples from different growth boules. The reflection is undetectable at all other energies, including the oxygen K edge jump, eliminating the possibility that it arises from a distortion in the crystal structure. In X-ray terminology, the peak responds to the anomalous scattering factors of the doped holes, and not those of the oxygen atoms, and therefore indicates a standing wave in the hole density without a (significant) lattice distortion. From its energy dependence and commensurate $5.00c_L$ periodicity, it is clear this modulation originates in the ladder substructure. The simplest interpretation is a crystallized state of holes in the ladder, which is almost degenerate with superconductivity but is stabilized under the set of parameters relevant to SCO.

To further characterize this reflection it was tracked through the L edge of copper ($2p \rightarrow 3d$ transition, Fig. 3), where it is also visible and notably still resides at $L_L = 0.2$, verifying that it disperses according to Bragg's law. Scattering at transition metal L edges is known to be sensitive to spin modulations[25,26], but close inspection reveals that it resonates not at the $L_{3/2}$ maximum but at the $L'_{3/2}$ shoulder, which arises from holes on the neighbouring ligands[27]. So the modulation has no obvious magnetic character.

Finally, the X-rays were tuned to the ladder MCP and L_L scans carried out at different temperatures (Fig. 4). The hole modulation is visible below $T_c \approx 250$ K and monotonically increases with cooling. The onset is gradual but close to the $T_c = 210$ K estimated from low-frequency dielectric spectroscopy[28], suggesting that the hole crystal is responsible for the CDW signatures in transport. The width of the reflection is temperature-independent even near the transition, so the correlation length is limited by some mechanism

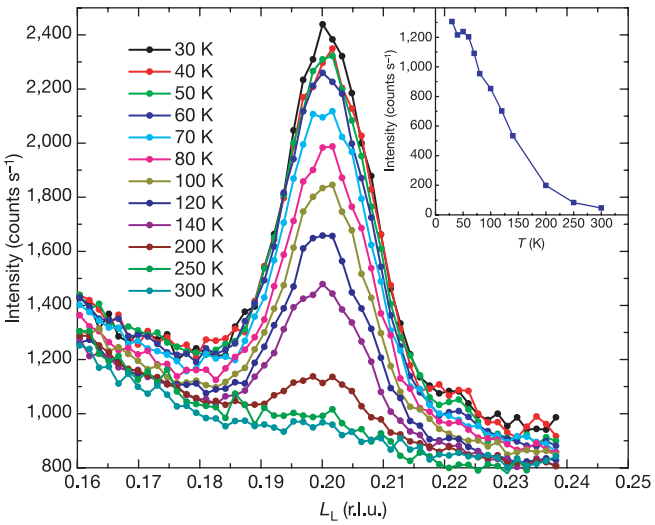

Figure 4 Temperature dependence of the hole crystal. The superlattice reflection becomes visible below $T = 250$ K. At its maximum (28 K), the peak count rate is 1,500 photons s^{-1} on a fluorescence background of 910 photons s^{-1}. The position and width of the peak are temperature-independent. Inset, integrated intensity of the peak as a function of temperature, showing gradual, crossover behaviour, in reasonable agreement with ref. 28.

other than thermodynamics, perhaps impurities[18] or intrinsic quantum fluctuations.

Our study of $Sr_{14}Cu_{24}O_{41}$ corroborates the prediction[4] of hole crystallization in doped ladders, and supports the picture that proximity to charge ordered states is a general property of superconductivity in copper oxides. RSXS does not permit precise determination of the form factor of the hole crystal, but no harmonic was seen at $L_L = 0.4$, suggesting a sinusoidal, delocalized modulation as discussed in ref. 7 rather than a fully localized Wigner crystal[29]. The peak width (Fig. 2) shows that the modulation is coherent across ~50 neighbouring ladders, demonstrating significant inter-ladder coupling.

As a hole crystal is charged, the reader may wonder why we do not see a distortion in the lattice which might be induced electrostatically. Such a modulation must exist, but would be of the order of the amplitude of the hole modulation itself, which is probably $\sim 10^{-2}$ electrons (ref. 7). By contrast, the density modulation of a structural Peierls CDW is of the order of the atomic number, Z. So the scattering power of a hole crystal is nominally weaker by $(10^{-2}/Z)^2 \approx 10^{-6}$. Our point is not that the structural modulation is truly zero, but that electronic correlations, rather than the electron–phonon interaction, drive the transition.

A significant open question concerns the relationship between the observed wavelength of $\lambda = 5.00c_L$ and the estimated[13] hole density in the ladder of $\delta = 0.057$ holes per copper atom. In models of hole crystallization[7,8], $\lambda = 1/\delta c_L$ or $2/\delta c_L$ in the strong and weak coupling regimes, respectively, which would require $\delta = 0.20$ or $\delta = 0.40$. These models neglect many residual interactions and details of the chemistry, but this relationship is resilient to such corrections. This may indicate a problem with estimates of δ, but it is worth noting that the hole crystal is commensurate with the lattice to within the measurement precision, suggesting that it is partly stabilized by elastic Umklapp processes. These can be significant for a commensurate hole crystal and perhaps strong enough to draw in extra charge from the chains. Another clue lies in the large transverse coherence length, which demonstrates significant inter-ladder interactions, and the relationship between λ and δ for a truly two-dimensional ordering pattern would not be so simple. It is therefore worth extending such models to the case of coupled ladders, or where the ladder interacts with a charge bath with which it may interchange carriers freely. □

Received 8 June; accepted 6 August 2004; doi:10.1038/nature02925.

1. Zaanen, J. & Gunnarsson, O. Charged magnetic domain lines and magnetism of high-T_c oxides. *Phys. Rev. B* **40,** R7391–R7394 (1989).
2. Löw, U., Emery, V. J., Fabricius, K. & Kivelson, S. A. Study of an Ising model with competing long- and short-range interactions. *Phys. Rev. Lett.* **72,** 1918–1921 (1994).
3. Tranquada, J. M., Sternlieb, J. D., Axe, J. D., Nakamura, Y. & Uchida, S. Evidence for stripe correlations of spins and holes in copper-oxide superconductors. *Nature* **375,** 561–564 (1995).
4. Dagotto, E., Riera, J. & Scalapino, D. Superconductivity in ladders and coupled planes. *Phys. Rev. B* **45,** 5744–5747 (1992).
5. Dagotto, E. & Rice, T. M. Surprises on the way from one- to two- dimensional quantum magnets: The ladder materials. *Science* **271,** 618–623 (1996).
6. Sigrist, M., Rice, T. M. & Zhang, F. C. Superconductivity in a quasi-one-dimensional spin liquid. *Phys. Rev. B* **49,** 12058–12061 (1994).
7. White, S. R., Affleck, I. & Scalapino, D. J. Friedel oscillations and charge density waves in chains and ladders. *Phys. Rev. B* **65,** 165122 (2002).
8. Carr, S. T. & Tsvelik, A. M. Superconductivity and charge-density waves in a quasi-one-dimensional spin gap system. *Phys. Rev. B* **65,** 195121 (2002).
9. Tranquada, J. M. *et al.* Coexistence of, and competition between, superconductivity and charge-stripe order in $La_{1.6-x}Nd_{0.4}Sr_xCuO_4$. *Phys. Rev. Lett.* **78,** 338–341 (1997).
10. Abbamonte, P. *et al.* A structural probe of the doped holes in cuprate superconductors. *Science* **297,** 581–584 (2002).
11. Fukuda, T., Mizuki, J. & Matsuda, M. Periodic hole structure in a spin-chain ladder material $Sr_{14}Cu_{24}O_{41}$. *Phys. Rev. B* **66,** 12104 (2002).
12. Etrillard, J., Braden, M., Gukasov, A., Ammerahl, U. & Revcolevschi, A. Structural aspects of the spin-ladder compound $Sr_{14}Cu_{24}O_{41}$. *Physica C* **403,** 290–296 (2004).
13. Nücker, N. *et al.* Hole distribution in $(Sr,Ca,Y,La)_{14}Cu_{24}O_{41}$ ladder compounds studied by x-ray absorption spectroscopy. *Phys. Rev. B* **62,** 14384–14392 (2000).
14. Uehara, M. *et al.* Superconductivity in the ladder material $Sr_{0.4}Ca_{13.6}Cu_{24}O_{41}$. *J. Phys. Soc. Jpn* **65,** 2764–2767 (1996).
15. Blumberg, G. *et al.* Sliding density-wave in $Sr_{14}Cu_{24}O_{41}$ ladder compounds. *Science* **297,** 584–587 (2002).
16. Gorshunov, B. *et al.* Charge-density wave formation in $Sr_{14-x}Ca_xCu_{24}O_{41}$. *Phys. Rev. B* **66,** 60508(R) (2002).
17. Kitano, H. *et al.* Microwave and millimeter wave spectroscopy in the slightly hole-doped ladders of $Sr_{14}Cu_{24}O_{41}$. *Europhys. Lett.* **56,** 434–440 (2001).
18. Grüner, G. *Density Waves in Solids* (Perseus, Cambridge, MA, 1994).
19. Motoyama, N., Osafune, T., Kakeshita, T., Eisaki, H. & Uchida, S. Effect of Ca substitution and pressure on the transport and magnetic properties of $Sr_{14}Cu_{24}O_{41}$ with doped two-leg Cu-O ladders. *Phys. Rev. B* **55,** R3386–R3389 (1997).
20. Matsuda, M. *et al.* Magnetic excitations and structural change in the S = 1/2 quasi-one-dimensional magnet $Sr_{14-x}Y_xCu_{24}O_{41}$ ($0 \le x \le 1$). *Phys. Rev. B* **56,** 14499–14504 (1997).
21. Cox, D. E. *et al.* Low-temperature charge ordering in $Sr_{14}Cu_{24}O_{41}$. *Phys. Rev. B* **57,** 10750–10754 (1998).
22. Hiroi, Z., Amelinckx, S., Van Tendeloo, G. & Kobayashi, N. Microscopic origin of dimerization in the CuO_2 chains in $Sr_{14}Cu_{24}O_{41}$. *Phys. Rev. B* **54,** 15849–15855 (1996).
23. Osafune, T., Motoyama, N., Eisaki, H. & Uchida, S. Optical study of the $Sr_{14-x}Ca_xCu_{24}O_{41}$ system: evidence for hole-doped Cu_2O_3 ladders. *Phys. Rev. Lett.* **78,** 1980–1983 (1997).
24. van Smaalen, S. Comment on "Periodic hole structure in a spin-chain ladder material $Sr_{14}Cu_{24}O_{41}$". *Phys. Rev. B* **67,** 26101 (2003).
25. Kao, C.-C. *et al.* Magnetic-resonance exchange scattering at the iron L_{II} and L_{III} edges. *Phys. Rev. Lett.* **65,** 373–376 (1990).
26. Dürr, H. A. *et al.* Chiral magnetic domain structures in ultrathin FePd films. *Science* **284,** 2166–2168 (1999).
27. Chen, C. T. *et al.* Out-of-plane orbital characters of intrinsic and doped holes in $La_{2-x}Sr_xCuO_4$. *Phys. Rev. Lett.* **68,** 2543–2546 (1992).
28. Vuletić, T. *et al.* Suppression of the charge-density-wave state in $Sr_{14}Cu_{24}O_{41}$ by calcium doping. *Phys. Rev. Lett.* **90,** 257002 (2003).
29. Wigner, E. On the interaction of electrons in metals. *Phys. Rev.* **46,** 1002–1011 (1934).

Acknowledgements We acknowledge J. Grazul and M. Sergent for help with sample polishing, and I. Affleck, J. B. Marston, Y.-J. Kim, P. M. Platzman, J. M. Tranquada, A. Tsvelik and T. M. Rice for discussions. This work was supported by the US Department of Energy, NWO (Dutch Science Foundation), and FOM (Netherlands Organization for Fundamental Research on Matter).

Competing interests statement The authors declare that they have no competing financial interests.

Correspondence and requests for materials should be addressed to P.A. (abbamonte@bnl.gov).

All-optical control of light on a silicon chip

Vilson R. Almeida, Carlos A. Barrios, Roberto R. Panepucci & Michal Lipson

School of Electrical and Computer Engineering, Cornell University, Ithaca, New York 14853, USA

Photonic circuits, in which beams of light redirect the flow of other beams of light, are a long-standing goal for developing highly integrated optical communication components[1–3]. Furthermore, it is highly desirable to use silicon—the dominant material in the microelectronic industry—as the platform for such circuits. Photonic structures that bend, split, couple and filter light have recently been demonstrated in silicon[4,5], but the flow of light in these structures is predetermined and cannot be readily modulated during operation. All-optical switches and modulators have been demonstrated with III–V compound semiconductors[6,7], but achieving the same in silicon is challenging owing to its relatively weak nonlinear optical properties. Indeed, all-optical switching in silicon has only been achieved by using extremely high powers[8–15] in large or non-planar structures, where the modulated light is propagating out-of-plane. Such high powers, large dimensions and non-planar geometries are inappropriate for effective on-chip integration. Here we present the experimental demonstration of fast all-optical switching on silicon using highly light-confining structures to enhance the sensitivity of light to small changes in refractive index. The transmission of the structure can be modulated by up to 94% in less than 500 ps using light pulses with energies as low as 25 pJ. These results confirm the recent theoretical prediction[16] of